SCIENCE IMMUNOLOGY | RESEARCH ARTICLE

AUTOIMMUNITY

Citrullination of NF-κB p65 promotes its nuclear localization and TLR-induced expression of IL-1β and TNFα

Bo Sun,[1,2]* Nishant Dwivedi,[1,2]* Tyler J. Bechtel,[3] Janet L. Paulsen,[4] Aaron Muth,[4] Mandar Bawadekar,[5] Gang Li,[1,2] Paul R. Thompson,[4] Miriam A. Shelef,[6] Celia A. Schiffer,[4] Eranthie Weerapana,[3] I-Cheng Ho[1,2]†

Many citrullinated proteins are known autoantigens in rheumatoid arthritis, a disease mediated by inflammatory cytokines, such as tumor necrosis factor–α (TNFα). Citrullinated proteins are generated by converting peptidyl-arginine to peptidylcitrulline, a process catalyzed by the peptidylarginine deiminases (PADs), including PAD1 to PAD4 and PAD6. Several major risk factors for rheumatoid arthritis are associated with heightened citrullination. However, the physiological role of citrullination in immune cells is poorly understood. We report that suppression of PAD activity attenuates Toll-like receptor–induced expression of interleukin-1β (IL-1β) and TNFα by neutrophils in vivo and in vitro but not their global transcription activity. Mechanistically, PAD4 directly citrullinates nuclear factor κB (NF-κB) p65 and enhances the interaction of p65 with importin α3, which brings p65 into the nucleus. The citrullination-enhanced interaction of p65 with importin α3 and its nuclear translocation and transcriptional activity can be attributed to citrullination of four arginine residues located in the Rel homology domain of p65. Furthermore, a rheumatoid arthritis–prone variant of PAD4, carrying three missense mutations, is more efficient in interacting with p65 and enhancing NF-κB activity. Together, these data not only demonstrate a critical role of citrullination in an NF-κB–dependent expression of IL-1β and TNFα but also provide a molecular mechanism by which heightened citrullination propagates inflammation in rheumatoid arthritis. Accordingly, attenuating p65-mediated production of IL-1β and TNFα by blocking the citrullination of p65 has great therapeutic potential in rheumatoid arthritis.

INTRODUCTION

Citrullination, also called deimination, is a form of posttranslational modification of proteins in which peptidylarginine residues are converted to citrulline. This process is mediated by peptidylarginine deiminases (PADs), including PAD1 to PAD4 and PAD6 (1), which have different tissue distributions and overlapping substrates (2). By converting positively charged arginine to neutral citrulline, citrullination can alter protein folding and function. Citrullination critically regulates early embryogenesis (3), pluripotency of stem cells (4), and epithelial-to-mesenchymal transformation of mammary cells (5).

Much less is known regarding the role of citrullination and the targets of PADs in hematopoietic cells, which mainly express PAD2 and PAD4. PAD4-mediated citrullination of histones is essential for the formation of neutrophil extracellular traps (NETs) (6). NETs are enriched with bactericidal proteins, such as LL37 and defensin, and can trap and kill invading bacteria. PAD4-deficient mice are more susceptible to bacterial infection in an animal model of necrotizing septic fasciitis (6). In addition, citrullination of extracellular proteins can modulate the function of the proteins and affect the behavior of immune cells. For example, PAD-citrullinated CXCL8 was less potent than native CXCL8 in attracting neutrophils after injecting into the peritoneum (7).

Citrullination also plays a pathogenic role in several human diseases. One of those diseases is rheumatoid arthritis (RA), which is characterized by the presence of anti-citrullinated protein antibodies and is mediated by inflammatory cytokines, such as tumor necrosis factor–α (TNFα), interleukin-1 (IL-1), and IL-6 (8). Several RA environmental and genetic risk factors are known to increase the activity or level of PADs. For example, smoking, a risk factor of RA, can increase the level of extracellular PAD2 and intracellular citrullinated proteins in lung lavage (9). In addition, the protein tyrosine phosphatase PTPN22 interacts with and suppresses the activity of PAD4 independently of its phosphatase activity (10). A C-to-T single-nucleotide polymorphism (SNP) located at position 1858 of human PTPN22 complementary DNA (cDNA) carries the highest risk of RA among all non–human leukocyte antigen genetic variations (11). This C1858T SNP, converting an arginine to a tryptophan, renders PTPN22 unable to interact with and suppress PAD4 activity, leading to cellular hypercitrullination (10).

How abnormal citrullination increases RA risk is still not understood. Existing data suggest that heightened citrullination expands the pool of citrullinated antigens and promotes the formation of NETs, which not only are a rich source of citrullinated antigens but also propagate joint inflammation (12). However, it is unclear if citrullination also intrinsically regulates other functions of immune cells in addition to promoting NETosis. If it does, what are the mechanisms of action?

Here, we report that inhibition of PADs in neutrophils results in a profound defect in Toll-like receptor (TLR)–induced expression of TNFα and IL-1β through suppressing nuclear factor κB (NF-κB) activity. We further characterize the molecular mechanism mediating the effect of PAD inhibition. Our data indicate that citrullination

[1]Division of Rheumatology, Immunology, and Allergy, Department of Medicine, Brigham and Women's Hospital, Boston, MA 02115, USA. [2]Harvard Medical School, Boston, MA 02115, USA. [3]Department of Chemistry, Boston College, Chestnut Hill, MA 02467, USA. [4]Department of Biochemistry and Molecular Pharmacology, University of Massachusetts Medical School, Worcester, MA 01605, USA. [5]Department of Medicine, University of Wisconsin–Madison, Madison, WI 53705, USA. [6]Department of Medicine, University of Wisconsin–Madison and William S. Middleton Memorial Veterans Hospital, Madison, WI 53705, USA.
*These authors contributed equally to this work.
†Corresponding author. Email: iho@partners.org

critically regulates the expression of inflammatory cytokines in neutrophils, in addition to promoting NETosis.

RESULTS

### Inhibition of LPS-induced transcription of inflammatory cytokines by suppressing PAD activity

To determine whether citrullination played a role in regulating the lipopolysaccharide (LPS)–induced expression of inflammatory cytokines, we pretreated primary human neutrophils with BB-Cl-amidine (BB-Cl), a pan-PAD inhibitor (13), before LPS stimulation, which is known to induce citrullination in neutrophils (14). Expectedly, the level of citrullinated histone H3 (cit-H3) was enhanced by LPS but reduced by BB-Cl (Fig. 1A). BB-Cl also inhibited LPS-induced transcription of IL-1β and TNFα in human neutrophils from three different donors (Fig. 1B). Dose-dependent inhibition by BB-Cl was also seen in mouse neutrophils (Fig. 1C). Near-complete inhibition was observed at 5 μM concentration, a dose that had no cytotoxic effect on neutrophils even after 8 hours of incubation or on the transcript level of a few housekeeping genes, such as *hypoxanthine-guanine phosphoribosyltransferase* (*HPRT*) (fig. S1, A and B), which are not

induced by LPS. BB-Cl also inhibited the induction of IL-1β and TNFα by other MYD88-dependent TLRs, such as Pam3CSK and flagellin (fig. S1, C and D). However, BB-Cl did not globally inhibit transcription because it had no effect on the granulocyte-macrophage colony-stimulating factor (GM-CSF)–induced expression of RhoH (Fig. 1D) and interferon-γ (IFNγ)–induced expression of IRF7 (Fig. 1E). Furthermore, BB-Cl did not alter leukotriene B4 (LTB4)–mediated transmigration (Fig. 1F), phorbol 12-myristate 13-acetate (PMA)–induced production of reactive oxygen species (ROS) (Fig. 1G), or bactericidal activity of neutrophils (Fig. 1H).

To examine the effect of BB-Cl on LPS-induced expression of IL-1β and TNFα in vivo, we injected wild-type (WT) mice with BB-Cl intraperitoneally 4 hours before an intraperitoneal LPS injection, which is known to cause infiltration of neutrophils into the lung (15). The infiltrating neutrophils also produce a large amount of IL-1β and TNFα, resulting in acute lung injury. We found that pretreatment with BB-Cl notably reduced the level of LPS-induced transcription of IL-1β and TNFα in the lung but did not affect the number of infiltrating neutrophils in bronchial lavage (Fig. 1I). Thus, BB-Cl inhibits LPS-induced transcription of IL-1β and TNFα in vitro and in vivo without broad effects on neutrophils.

Fig. 1. Inhibiting LPS-induced expression of TNFα and IL-1β by BB-Cl. (**A** to **E**) Primary human (A and B) or mouse (C to E) neutrophils were stimulated with LPS (A to C), GM-CSF (D), or IFNγ (E) in the absence or presence of indicated concentrations of BB-Cl for 2 hours. Whole-cell extract was analyzed by Western blotting for the levels of cit-H3 and total histone H3 (H3) (A). The transcript levels of indicated genes were quantified with real-time PCR in duplicate (B to E). Data in (B) are from three different donors. (**F**) Mouse neutrophils (2 × 10^5 cells) were pretreated with BB-Cl in the upper chambers of transwells and then allowed to migrate toward LTB4 (100 nM) in the bottom chambers for 1 and 2 hours. The numbers of neutrophils in the bottom chambers from one of the two triplicate experiments are shown. (**G**) Mouse neutrophils were stimulated with PMA in the presence or absence of BB-Cl pretreatment.

The generation of ROS was quantified. (**H**) Mouse neutrophils were subjected to in vitro bactericidal assay with or without BB-Cl pretreatment. The survival of bacteria from one of the two triplicate experiments is shown. (**I**) Mice (five mice per group) were subjected to LPS-induced lung injury with or without BB-Cl pretreatment. The transcript level of IL-1β and TNFα in lung homogenate was quantified with real-time PCR (left and middle panels). The numbers of neutrophils in bronchial lavage are shown in the right panel. The data shown are from one of two experiments.
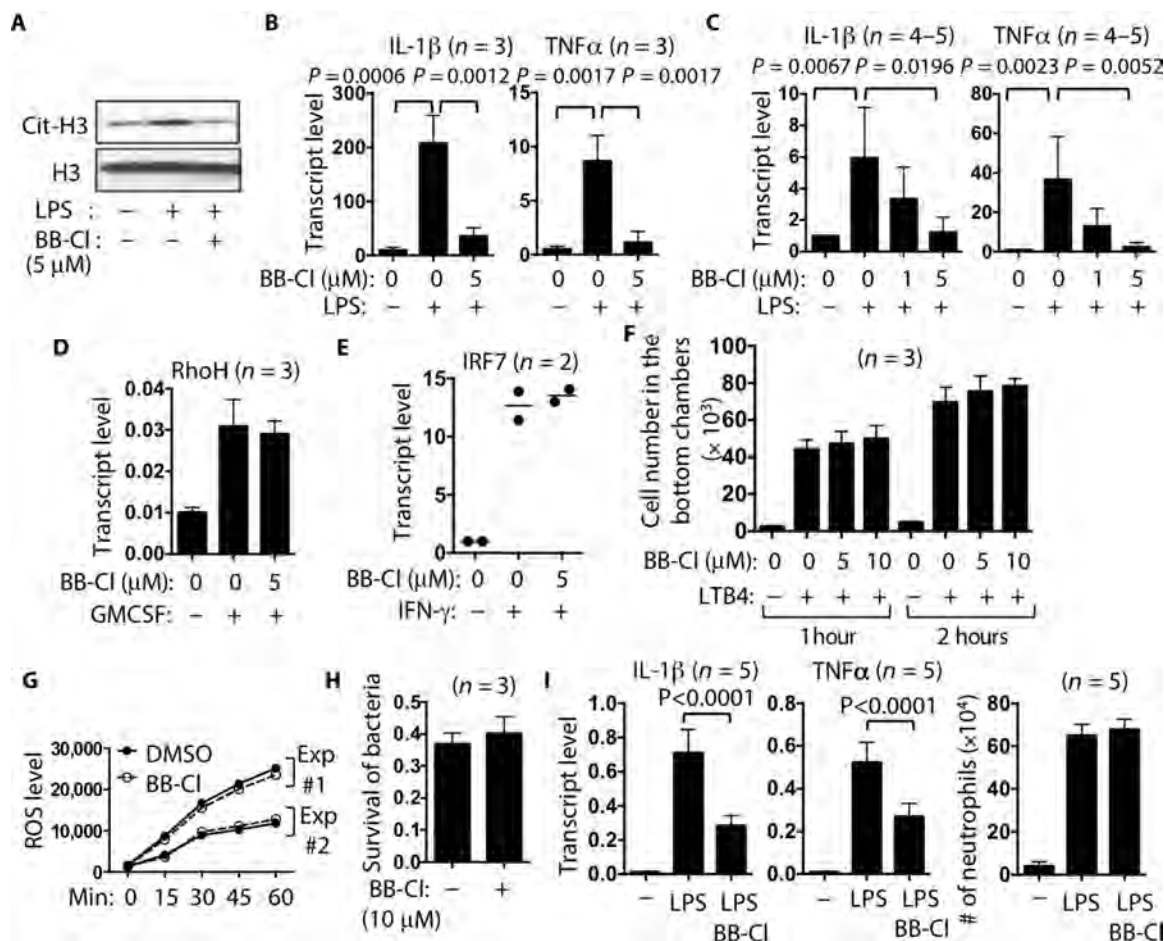
Because BB-Cl is a pan-PAD inhibitor, we investigated whether a single PAD was required for LPS-induced IL-1β or TNFα expression or whether the PADs are functionally redundant. Neutrophils express the highest level of PAD4 among hematopoietic cells and also express PAD2 and PAD3 (fig. S2A) (*2*), but we saw no defect in the expression of IL-1β or TNFα in LPS-stimulated PAD4-deficient (KO) or PAD2KO bone marrow neutrophils (fig. S2B), suggesting functional redundancy.

Enhancement of NF-κB activity by the enzymatic activity of PADs

LPS-induced expression of TNFα and IL-1β depends on NF-κB. We therefore used HL60 cells in transient transfection assays to examine the effect of citrullination on NF-κB activity. HL60 are human promyelocytic leukemia cells, which can be differentiated to granulocyte-like cells [tentatively called differentiated HL60 (dHL60)] with dimethyl sulfoxide (DMSO). As expected, LPS treatment of dHL60 cells induced the expression of TNFα and IL-1β, and their induction was blocked by BB-Cl (Fig. 2A). By contrast, BB-Cl had no effect on IFNγ-induced expression of IRF7 in dHL60 (Fig. 2B). A recent study showed that bacterial DNA also induces IL-1β expression in neutrophils through the Sox5–NF-κB pathway (*16*). In agreement with this observation, transfection of dHL60 with plasmid DNA induced the expression of IL-1β and TNFα in a BB-Cl–sensitive manner (Fig. 2C).

We then pretreated dHL60 with BB-Cl and transfected the pretreated cells with a reporter driven by NF-κB binding sites. We found that BB-Cl suppressed the transcriptional activity of NF-κB in a dose-dependent manner (Fig. 2D). By contrast, the activity of a reporter driven by CRE (cyclic adenosine monophosphate response element) or NFAT (nuclear factor of activated T cells) sites, which had basal activity comparable with or slightly lower than that of the NF-κB reporter, was not inhibited by BB-Cl. To ensure that our findings were not an off-target effect of BB-Cl and to further examine whether PAD activity influenced NF-κB activity, we cotransfected dHL60 cells with the NF-κB reporter and an expression vector containing PAD4, the dominant PAD in neutrophils and dHL60 cells. We found that forced expression of PAD4 increased NF-κB activity in a dose-dependent manner but had no effect on the activity of the CRE or NFAT reporter (Fig. 2, E and F). Furthermore, a mutant PAD4, which contains a C645S mutation and is enzymatically less active (*5*), is less potent in enhancing NF-κB activity (Fig. 2F). Together, our data indicate that the enzymatic activity of PAD4 enhances the activity of NF-κB.

Inhibition of nuclear localization of NF-κB p65 by BB-Cl

Citrullination of histones can epigenetically influence gene expression (*17*). However, plasmid DNA, such as the NF-κB reporter, is not integrated into chromatin in the transient transfection assay. Thus, the impact of BB-Cl on NF-κB activity is unlikely to be due to alterations in the status of histone citrullination. LPS activates the canonical NF-κB pathway, in which MYD88, TRAF6, and the IKK [inhibitor of NF-κB (IκB) kinase] complex are sequentially activated, eventually leading to the phosphorylation and degradation of IκB. Degradation of IκB frees p65/p50 dimers, which are then brought into the nucleus by importins. We found that pretreatment with BB-Cl had no impact on LPS-induced degradation of IκB in primary human neutrophils (Fig. 2G). We then examined the level of nuclear p65, which was barely detectable in the nucleus of unstimulated primary human neutrophils. Nuclear p65 became clearly visible 30 min after LPS stimulation, and its level peaked at 1 hour (Fig. 2H). However, pretreatment with BB-Cl reduced the level

of nuclear p65 by at least 50% in all time points examined. By contrast, BB-Cl had no impact on the total level of p65 or regeneration of IκB after LPS stimulation (Fig. 2G). The effect of BB-Cl on LPS-induced nuclear localization of p65 was also observed in dHL60 cells by immunocytochemistry (Fig. 2I and fig. S3).

Physical interaction between p65 and PAD4

To determine whether PAD activity regulates the nuclear localization of p65, we tested if p65 physically interacted with PAD4 by coimmunoprecipitation using anti-p65. Anti-p65, but not control immunoglobulin G (IgG), was able to immunoprecipitate a 74-kDa protein that was recognized by anti-PAD4 from unstimulated primary human neutrophils (Fig. 3A). The coimmunoprecipitation of p65 and PAD4 was diminished upon LPS stimulation but was partially preserved by BB-Cl. Reciprocally, glutathione *S*-transferase (GST)–fused PAD4, but not GST, was able to pull down exogenous p65 expressed in 293T cells (Fig. 3B).

To map the structural domains that are required for the interaction between PAD4 and p65, we overexpressed full-length or various truncation mutants of p65 in 293T cells (Fig. 3C) and used GST-PAD4 to trap the overexpressed p65 from 293T cell extract. We found that fragments 1–190 (p65-N), 191–384 (p65-M), and 1–384 (p65-N+M) strongly interacted with PAD4 than did full-length p65. By contrast, fragment 286–551 (p65-C) was not pulled down by PAD4 at all. Deletion of 1–190 (p65-M+C) or 191–285 (p65-N+C) had little effect on the interaction between p65 and PAD4. These data suggest that p65 interacts with PAD4 through two independent domains: 1–190 and 191–285. Either one is sufficient to mediate the interaction between p65 and PAD4. Both domains fall within the Rel homology domain (RHD) that is also critical for DNA binding and dimerization of p65.

Conversely, we used GST-tagged p65 to pull down full-length PAD4 and a series of PAD4 truncation mutants expressed in 293T cells. We found that amino acid residues 1 to 119 (PAD4-N) interacted with p65 much more strongly than did full-length PAD4 (Fig. 3D). Deletion of 1–119 (PAD4-M+C) modestly reduced the interaction between PAD4 and p65. Fragment 120–523 (PAD4-M) was also pulled down by GST-p65 as efficiently as full-length PAD4. These results suggest that either 1–119 or 120–523 is sufficient to mediate the interaction between PAD4 and p65. However, 1–119 is very likely the dominant interacting domain.

Impacts of an RA-prone haplotype of *PADI4* on NF-κB activity

A haplotype of *PADI4* (called type 1 haplotype), encoding a PAD4 protein having three missense mutations (S55G/A82V/A112G, called SNP-PAD4), is associated with a higher risk of RA (*18*). These three mutations are located at the N terminus of PAD4, far away from its enzymatic domain, and do not have a significant effect on the intrinsic catalytic activity of PAD4 (*19*, *20*). The observation that p65 interacts mainly with the N terminus of PAD4 prompted us to propose that the S55G/A82V/A112G may affect the interaction between PAD4 and p65. We therefore expressed WT or SNP-PAD4 in 293T cells and then used GST-p65 to pull down the exogenous WT or SNP-PAD4 protein. We found that exogenous SNP-PAD4 was more efficiently pulled down by GST-p65 than by WT PAD4 (Fig. 3E). In addition, SNP-PAD4 enhanced NF-κB activity more robustly than did WT PAD4 in the luciferase reporter assay (Fig. 3F). At a low dose (1.5 μg), SNP-PAD4 is almost twice as effective as WT PAD4 in boosting the activity of NF-κB. Our data suggest that the three missense mutations increase

Fig. 2. BB-Cl inhibits nuclear localization of NF-κB p65. (A and **B**) dHL60 cells were stimulated with LPS (A) or IFNγ (B) for 2 hours in the presence or absence of BB-Cl pretreatment. The expression of the indicated genes was quantified with real-time PCR. (**C**) dHL60 cells were pretreated with BB-Cl and then transfected with empty plasmid vectors. The transcript levels of IL-β and TNFα were quantified with real-time PCR 4 hours later. (**D**) dHL60 cells were pretreated with BB-Cl and then transfected with an NF-κB, CRE, or NFAT luciferase reporter. The normalized luciferase activities were measured 4 hours later. (**E** and **F**) dHL60 cells were transfected with indicated amounts [6 μg in (E)] of an expression vector of His-tagged WT PAD4 (E and F), mutant PAD4 (F), or the corresponding empty vector (E) along with indicated reporters [NF-κB reporter in (F)]. The normalized luciferase activities were measured 4 hours later. The levels of exogenous PAD4 and endogenous tubulin in the transfected cells were also analyzed by Western blotting (F). (**G** and **H**) Primary human neutrophils were pretreated with 10 μM BB-Cl for 40 min and then stimulated with LPS for the indicated periods of time. Whole-cell (G) and nuclear (H) extracts were prepared separately and examined by Western blotting using the indicated antibodies. The density of IκB in whole-cell extract (G) and p65 in nuclear extract (H) was normalized against that of tubulin and histone H3 (H3). (**I**) dHL60 cells were left unstimulated or stimulated with LPS in the presence or absence of BB-Cl pretreatment. The cells were stained with anti-p65 (in red) and Draq5 (in blue) and visualized with a confocal microscope. The mean intensity of nuclear p65 in 12 to 13 individual fields (four to five cells per field) from two independent experiments is shown in the bar graph. ns, not significant.


the expression of IL-1β and TNFα by strengthening the interaction between PAD4 and p65.

Modeling the physical interaction between PAD4 and p65

Our data indicate that PAD4 interacts mainly with the RHD of p65, which is divided into the DNA binding domain and the dimerization domain. The crystal structures of PAD4 [Protein Data Bank (PDB) ID, 4DKT] and the RHD of p65 (PDB ID, 2I9T) have been separately solved. We therefore used BioLuminate to model the PAD4/p65 complex. The biological unit of PAD4 is thought to be a dimer, which was used as the receptor. The top 1000 of 70,000 poses were retained and clustered by similarity of structural orientation. The top 30 clusters were evaluated. Eight of the 30 clusters showed interaction with the N terminus of PAD4. The first cluster of the 8 (the 15th most populated of the 30) showed that the DNA binding domain of p65 interacts with the N terminus of one PAD4, whereas the dimerization domain of p65 interacts with the midregion of another PAD4 (Fig. 4A). The docked model is consistent with the data showing that there are two potential interaction points between PAD4 and p65 (Fig. 3, C and D). Models within this cluster also show favored hydrophobic contacts between A82 of PAD4 and P168 of p65, with distances between 3.2 and 4.8Å (Fig. 4B). The docked model predicts that the A82V mutation encoded by the type 1 haplotype of *PADI4* will lead to more favorable hydrophobic contacts between residue 168 of p65 and residue 82 of PAD4, suggesting a stronger association between PAD4 and p65, whereas the A112G in close contact with A82V would alter the flexibility in the region. This prediction is consistent with the data shown in Fig. 3E.

Detection of citrullinated p65

One potential mechanism by which PAD4 regulates the activity of NF-κB is by citrullinating p65. We therefore set to determine if citrullinated p65 (cit-p65) was present intracellularly. We stimulated dHL60 cells with LPS in the absence or presence of BB-Cl. Whole-cell extract was labeled with biotin-phenylglyoxal (PG), a chemical probe that specifically binds to peptidylcitrulline under acidic conditions (*21*). The biotin-
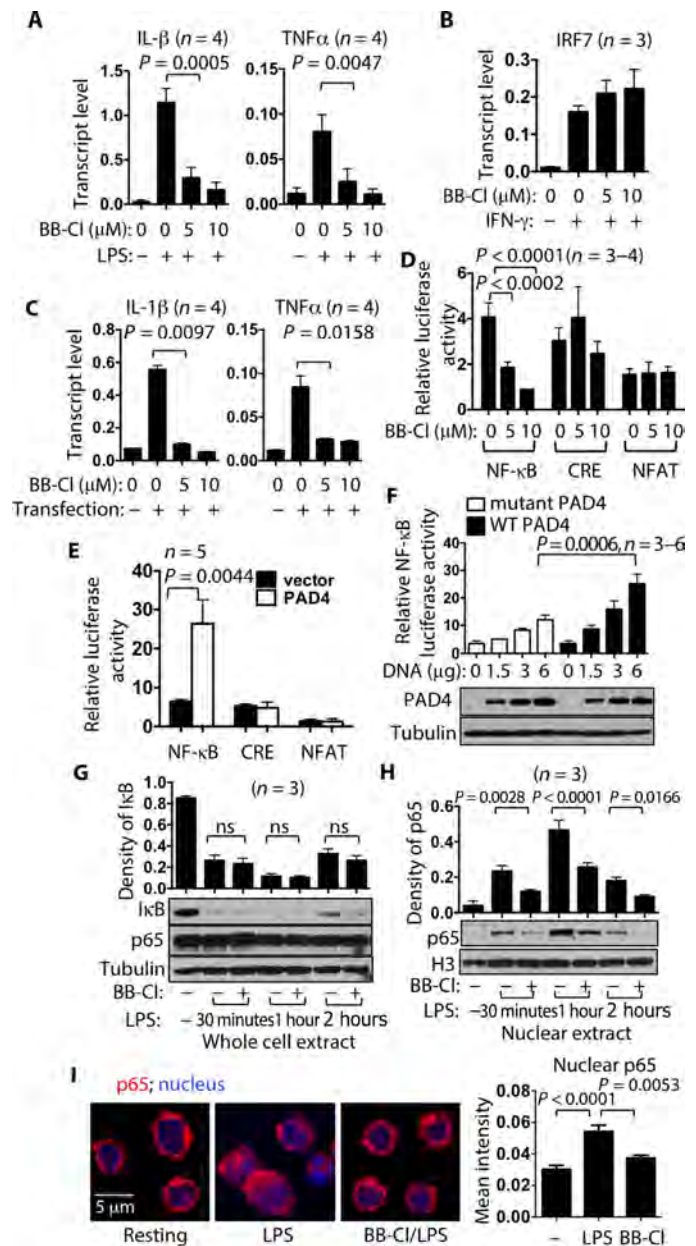
PG–labeled proteins were pulled down with streptavidin-agarose beads and then examined by Western blotting. When we probed the pulldown extract with anti-H3, we found that the level of H3 was increased by more than twofold after LPS stimulation (Fig. 5A). This increase was suppressed by BB-Cl. This pattern was almost identical to what is shown in Fig. 1A, validating this approach to detect intracellular citrullinated proteins. We then probed the pulldown extract with anti-p65. A protein band of about 65 kDa was detected in extracts from LPS-stimulated cells but not in unstimulated cells (Fig. 5B). The level of this protein band was reduced by BB-Cl. This result demonstrates that p65 is citrullinated in LPS-stimulated dHL60 cells and that its citrullination is inhibited by BB-Cl.

We subsequently performed in vitro citrullination to confirm that p65 is a direct substrate of PAD4. We generated GST-p65 and enriched
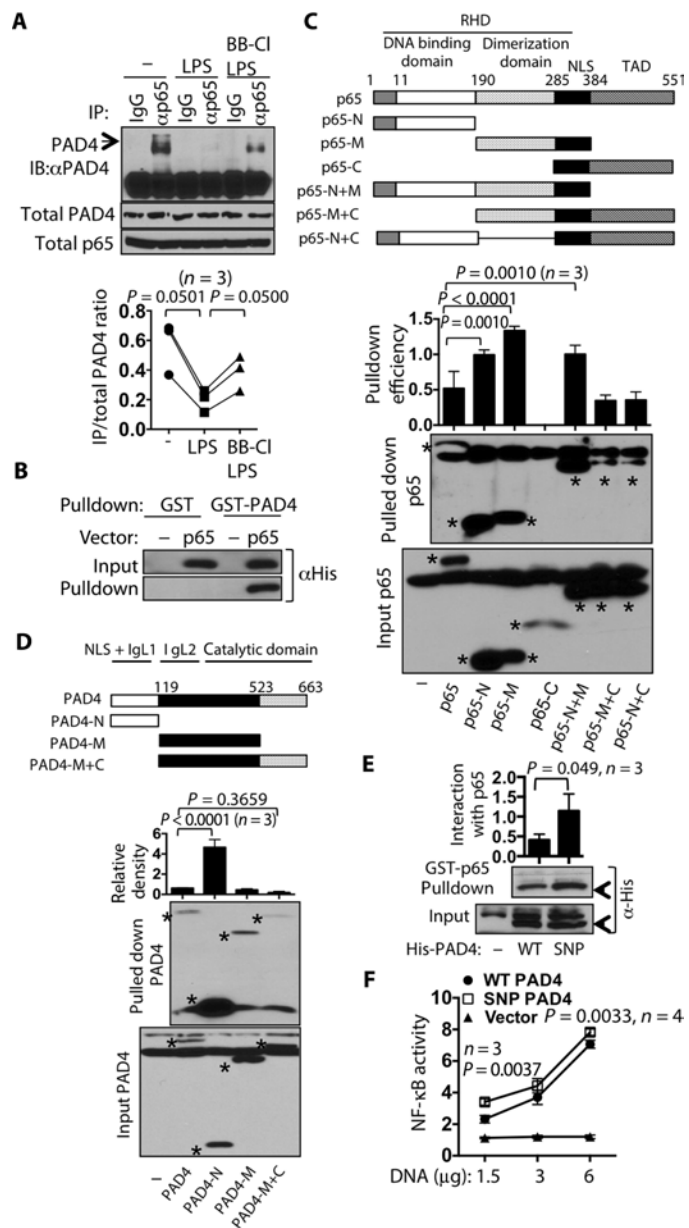
Fig. 3. Physical interaction between PAD4 and p65. (**A**) Primary human neutrophils were stimulated with LPS with or without BB-Cl pretreatment. Whole-cell extract was subjected to immunoprecipitation (IP) with anti-p65 or control IgG. The immunoprecipitant was probed with anti-PAD4. A fraction of the unmanipulated whole-cell extract was probed with anti-PAD4 and anti-p65 (total). The normalized density of precipitated PAD4 is shown in the bottom bar graph. (**B**) GST or GST-PAD4 was used to pull down His-tagged p65 expressed in 293T cells. Whole-cell extract from the transfected 293T cells (top panel) and pulldown extract (bottom panel) were probed with anti-His. (**C** to **E**) GST-PAD4 (C) or GST-p65 (D and E) was used to pull down His-p65 (C), His-PAD4 (D and E), or His–SNP-PAD4 (E) expressed in 293T cells. Whole-cell extract from the transfected 293T cells (input) and pulldown extract were probed with anti-His. Schematic diagrams of the truncation mutants are shown at the top panels of (C) and (D). The asterisks in the Western blots of (C) and (D) mark exogenous His-p65 (C) or His-PAD4 (D). The arrowheads in (E) mark His-PAD4 and His–SNP-PAD4. The normalized density of pulldown His-p65 (C), His-PAD4 (D and E), and His–SNP-PAD4 (E) is shown in the bar graphs. (**F**) dHL60 cells were transfected with the indicated amounts of vectors expressing WT PAD4 or SNP-PAD4 along with the NF-κB reporter. The normalized luciferase activity was measured 4 hours later.

the protein on glutathione beads (Fig. 5C, left panel). Purified GST-p65 was incubated with PAD4 and then probed with F95, a mouse monoclonal IgM raised against a deca-citrullinated peptide (*22*). Several dense F95-reactive bands were detected in PAD4-treated GST-p65 but not in untreated GST-p65 (Fig. 5C, right panel). By contrast, there was little or no F95 reactivity of PAD4-treated GST, confirming that GST-p65 is a direct substrate of PAD4.

Identification of citrullination sites within p65

The purified GST-p65 protein contains several degradation products. Because GST was fused at the N-terminal end of p65, these degradation products are the result of truncations in the C terminus of p65. The degradation products actually correlated with several major groups of citrullinated GST-p65 (cit–GST-p65): 30, 35, and 50 to 80 kDa (schematic diagrams on the right of Fig. 5D). The observation that the degraded GST-p65 products are also citrullinated suggests the presence of citrullination sites within the N terminus of p65. There are five arginines (R30, R33, R35, R41, and R50) within the first 50 amino acid residues of p65. We therefore converted each of the arginines to a lysine (Fig. 5D, left panel), which maintains the positive charge but cannot be citrullinated, and subjected the mutants to in vitro citrullination. We then examined the effect of the R-to-K mutation on the level of 50- to 80-kDa cit–GST-p65, the dominant species. R30K, R33K, and R41K mutations had little impact on the density of the 50- to 80-kDa forms of cit–GST-p65. By contrast, R50K mutation and, to a lesser degree, R35K mutation modestly attenuated the level of citrullination (Fig. 5D, middle). A mutant containing both R35K and R50K mutations (R35/50K) was still citrullinated to about 50% of the WT level (Fig. 5, E and F), suggesting the presence of additional citrullination sites.

To identify additional citrullination sites beyond the N terminus of p65, we prepared native and in vitro cit–GST-p65 and performed in-gel digestion and high-resolution liquid chromatography–tandem mass spectrometry (LC-MS/MS) analysis on the ~80-kDa bands (fig. S4). The citrullinated forms of the two peptides, INGYTGPGTVRISLVTK (containing R73) and IQTNNNPFQVPIEEQRGDYDLNAVR (containing R149), were identified with higher spectral counts in cit–GST-p65 compared with native GST-p65 (table S1 and Fig. 6A). Manual interrogation of the high-resolution MS1 spectra confirmed the presence of the ~1-Da heavier citrullinated species for each of these peptides (Fig. 6A). The lack of the corresponding monoisotopic peak for the uncitrullinated peptide within the isotope envelope confirmed the assignments of these citrullinated species (Fig. 6A). Generation of high-resolution MS2 fragmentation spectra localized the site of citrullination to R73 and R149 based on the presence of matching y6 and y7 pairs for the R73 peptide and b15 and b16 pairs for the R149 peptide. In each case, the high-resolution fragment masses unambiguously confirmed the presence of a citrulline residue based on the ~1-Da mass shift.

However, conversion of R73 and/or R149 to lysine also only modestly reduced the citrullination of p65 (Fig. 6B). We therefore created a R35K/R50K/R73K/R149K quadruple mutant (4R-K) and found that this mutant was much more resistant to PAD4-mediated citrullination; this mutant was citrullinated to only 20% of the WT level (Fig. 6, C and D). One possible explanation for the reduced citrullination was that the 4R-K mutation interfered with the interaction between p65 and PAD4. According to the model shown in Fig. 4, these four arginine residues do not participate in the p65/PAD4 interaction. In addition, the 4R-K mutant still physically interacted with PAD4 as tightly as WT p65 in GST
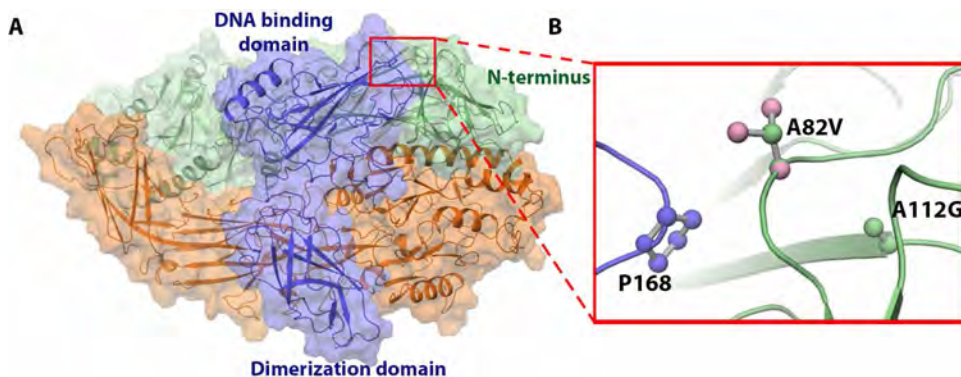
Fig. 4. Computer modeling of the p65/PAD4 interaction. (**A**) Docking model of the PAD4 dimer (individual monomers shown in green and orange) with p65 (DNA binding and dimerization domains; purple). The model shows an interface between the N terminus of PAD4 and the DNA binding domain of p65, whereas the dimerization domain of p65 interacts with the adjacent PAD4. (**B**) The interfacial regions between PAD4 (green) and p65 (purple) indicate an interaction between P168 in the DNA binding domain of p65 with A82 in the N terminus of PAD4. A82 and A112 are in close contact. The V82 encoded by the type 1 haplotype of *PADI4* is modeled in pink.

pulldown assay (fig. S5), suggesting that its resistance to citrullination is not due to weakened interaction with PAD4. Instead, our data demonstrate that R35, R50, R73, and R149 are the major, but not the only, in vitro citrullination sites of p65.

Citrullination of p65 promotes its interaction with importin α3

Our data so far suggest that citrullination of p65 facilitates its nuclear localization. To determine whether cit-p65 was present in the nucleus, we separately prepared cytoplasmic and nuclear extract from primary human neutrophils. Cit-p65 was pulled down with biotin-PG and detected with anti-p65 according to the method described in Fig. 5B. We detected cit-p65 in both cytoplasmic and nuclear extract only in LPS-stimulated cells, but not in resting or BB-Cl–treated cells (Fig. 7A). Because the rate of disappearance of nuclear p65 after LPS stimulation was very comparable between BB-Cl–treated and untreated cells (Fig. 2H), we postulated that citrullination regulated mainly the nuclear entry of p65 but not its nuclear export by IκB or degradation by the proteasome. The nuclear entry of p65 is mediated by importin α3 (*23*). We therefore postulated that citrullination of p65 facilitated its interaction with importin α3. In agreement with published data, anti–importin α3 was able to coimmunoprecipitate p65 from LPS-stimulated primary human neutrophils and dHL60 cells (Fig. 7B). This coimmunoprecipitation was attenuated by BB-Cl. Conversely, in vitro cit–GST-p65 was more efficient than native GST-p65 in pulling down importin α3 from dHL60 cells (Fig. 7C). No importin α3 was pulled down by native or PAD4-treated GST. Citrullination neutralizes the positive charge of arginine and might affect the binding of p65 to DNA. We found that cit–GST-p65, but not PAD4-treated GST, bound to the NF-κB site of the IL-1β promoter as well as, if not better than, native GST-p65 (fig. S6). By contrast, cit–GST-p65 did not bind to a control sequence that does not contain a consensus NF-κB site.

We then examined if citrullination of R35, R50, R73, and/or R149 is responsible for the enhanced interaction between cit–GST-p65 and importin α3. We found that native WT GST-p65, R35K, R50K, R73K/R149K, and 4R-K mutants all interacted weakly and comparably with importin α3 (Fig. 7D). Citrullination of WT GST-p65, R35K, R50K, and R73K/R149K comparably increased their interaction with importin α3 in the GST

pulldown assay. However, no such increase was observed in citrullinated 4R-K mutant. Furthermore, 4R-K mutant was less efficient than WT p65 in transactivating the NF-κB reporter in dHL60 cells (Fig. 7E).

DISCUSSION

In summary, we have demonstrated that NF-κB p65 is a direct substrate of PAD4 in neutrophils. TLR-induced citrullination of p65 at four arginine residues located at its N terminus augments its interaction with importin α3 and nuclear localization and, consequently, the expression of IL-1β and TNFα. Furthermore, the three missense mutations encoded by the type 1 haplotype of *PADI4* strengthen the interaction between PAD4 and p65, thereby enhancing NF-κB activity. Thus, our data have expanded the role of protein citrullination in neutrophils beyond facilitating the formation of NETs.

Several studies have also suggested a role for citrullination in promoting inflammation. Rabadi *et al.* (*24*) recently reported that PAD4KO mice were more resistant to ischemic renal injury due to attenuated expression of several NF-κB–dependent inflammatory cytokines, including MIP-2 and TNFα. They further showed that overexpression of PAD4 in mouse proximal renal tubule cells promoted nuclear localization of NF-κB p65. Although the mechanism of this finding was not investigated, PAD4-mediated citrullination of p65 may increase its interaction with importins in proximal renal tubule cells.

Sharma *et al.* (*25*) demonstrated that PAD4 small interfering RNA or Cl-amidine, another pan-PAD inhibitor, attenuated the transcription of TNFα in MCF7 breast cancer cells. They proposed that citrullination of R8 of histone H3 weakens the binding of transcriptional repressor HP1a to trimethylated K9 of histone H3, thereby epigenetically augmenting the transcription of TNFα. This mechanism very likely also operates in neutrophils and is consistent with several reports demonstrating that histones are targets of PAD2 and PAD4. However, this epigenetic mechanism should not affect nuclear localization of p65. In addition, the transient transfection assay shown in Fig. 2 (E and F) is not subjected to epigenetic regulation. Furthermore, Ghari *et al.* (*26*) showed that citrullination of the transcription factor E2F facilitated its binding with BRD4 (bromodomain-containing protein 4) and recruitment to the promoter of several inflammatory cytokine genes, including *IL-1β* and *TNFα*, thereby augmenting the expression of these cytokines. Thus, citrullination can regulate the expression of IL-1β and TNFα by more than one mechanism: epigenetically modifying their genetic loci, facilitating the recruitment of E2F to their promoters, and promoting the nuclear translocation of p65. This scenario could also explain why BB-Cl nearly shuts down the transcription of IL-1β and TNFα but reduces the level of nuclear p65 only by 50% (Fig. 2H).

In contradiction to the aforementioned data, Lee *et al.* (*27*) reported that PAD2 physically interacted with IKKγ and that overexpression of PAD2 modestly inhibited LPS-induced NF-κB activity in RAW 264.7 cells. There are several possible explanations for the discrepancy. Overexpression of PAD2 may lead to citrullination of
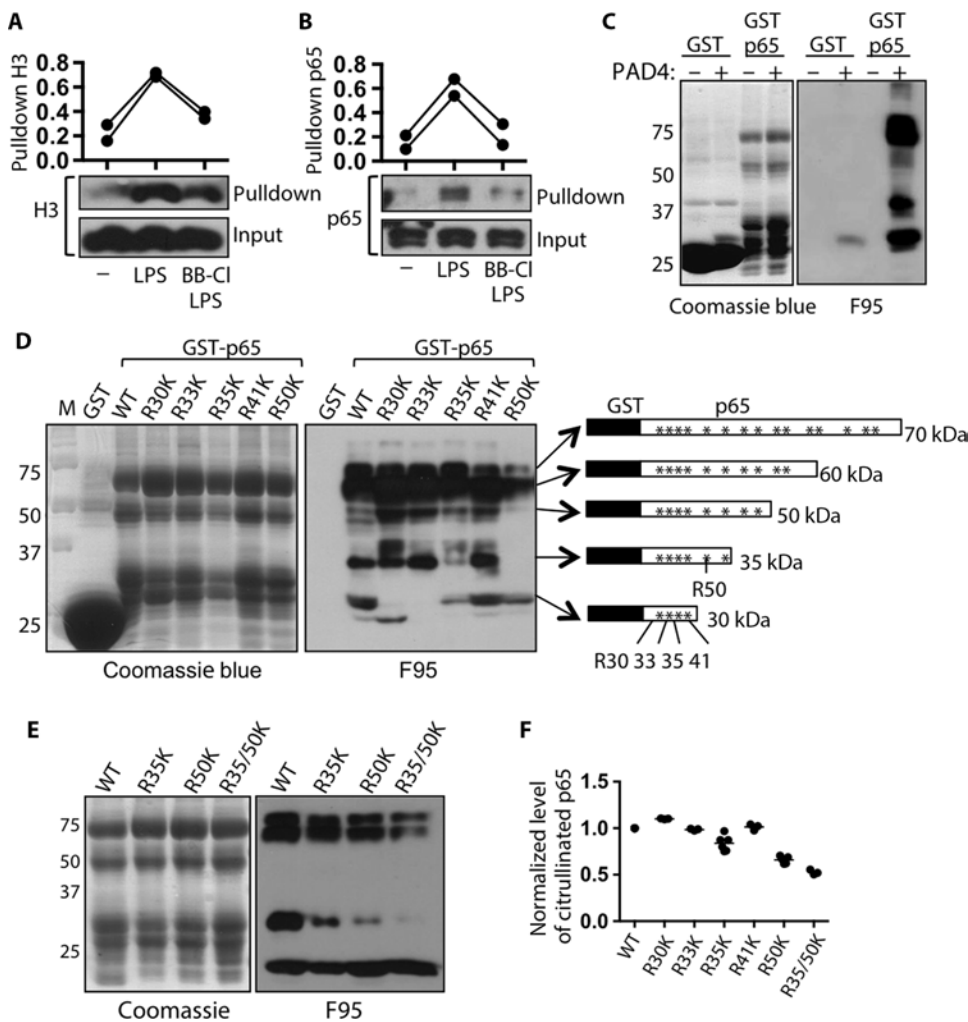
Fig. 5. Detection of cit-p65. (**A** and **B**) Whole-cell extract from dHL60 cells stimulated with LPS in the presence or absence of BB-Cl pretreatment was labeled with biotin-PG probe, pulled down with streptavidin beads, and probed with anti–histone H3 (H3) (A) or anti-p65 (B) by Western blotting (pulldown). A fraction of the biotin-PG–labeled extract before pull down was also analyzed to serve as input controls. The normalized density of pulldown H3 or p65 from two experiments is shown in the dot graphs. Data from the same experiment are connected with lines. (**C** to **E**) Recombinant GST, GST-p65, and various R-to-K mutants were incubated with (C to E) or without (C) PAD4, fractionated by SDS–polyacrylamide gel electrophoresis (PAGE) gels, stained with Coomassie blue (left panels), or probed with F95 (C and E, right panels, and D, middle panel) by Western blotting. Schematic diagrams of predicted recombinant GST-p65 proteins are shown at the right panel of (D). Arginine residues are marked with asterisks. The diagrams and the location of the arginine residues are not to scale. (**F**) The density of the citrullinated 50- to 80-kDa bands detected with F95 was normalized against that of the corresponding bands detected with Coomassie blue. The normalized density of citrullinated WT GST-p65 was arbitrarily set as 1. Cumulated results from all experiments are shown. Each dot represents one experiment.

peptidylarginines that are not targets of PAD2 under physiological conditions. Our approach of pharmacologically suppressing PAD activity is less likely to cause such artifacts. Unlike other hematopoietic cells, such as monocytes and lymphocytes, neutrophils express a very high level of PAD4. Thus, the functional impact of PADs in RAW 264.7 macrophage–like cells may differ from that in neutrophils and HL60 cells. Last, BB-Cl has no effect on the degradation of IκB (Fig. 2G), the downstream event of IKK activation. Thus, the functional significance of IKKγ citrullination is still unclear.

The type 1 haplotype of *PADI4* encoding SNP-PAD4 is associated with a higher risk of RA (*18*). The S55G/A82V/A112G SNP does not affect the intrinsic enzymatic activity of PAD4 but stabilizes the PAD4 transcript (*18–20*). However, we found that exogenous WT and SNP-PAD4 proteins reached comparable levels when expressed in dHL60 cells, a finding that somewhat argues against the published data. Instead, our data depict an attractive model for the S55G/A82V/A112G mutation to modulate the function of PAD4. By strengthening the interaction between PAD4 and p65, this haplotype results in an enhancement of p65 activity. SNP-PAD4 was also shown to preferentially interact with HDAC1, adding another layer to how this mutant might regulate gene expression (*20*).

Several issues remain to be clarified. Although our in vitro data have demonstrated that citrullination of p65 promotes its nuclear localization, it is unclear how citrullination at R35, R50, R73, and R149 enhances p65/importin α3 interaction. It also remains to be determined if the four arginine residues are the major sites when citrullination of p65 takes place in primary neutrophils, and even if so, the in vivo functional impact of those citrullination events is still unknown. In addition, we were unable to demonstrate an essential role for PAD4 or PAD2 in promoting the expression of IL-1β and TNFα, possibly due to functional redundancy among PADs. Unfortunately, mice deficient in both PAD2 and PAD4 have not been generated by crossing PAD2KO and PAD4KO mice due to the close proximity of these two genes in the mammalian genome. Last, it should be noted that the proposed crystal structure of the p65/PAD4 dimer is modeled from the existing crystal structure of p65 and PAD4.

Our data prompt us to look at the role of protein citrullination in immune cells in a new light. In addition to structural proteins and histones, the function of transcription factors is probably also subject to regulation by citrullination; each citrullination event very likely has a unique functional consequence. Thus, the functional role of protein citrullination can be as important and complicated as other forms of posttranslational modifications, such as phosphorylation. Our data also have important implications in the pathogenesis of RA. Several major risk factors of RA are associated with local or systemic hypercitrullination (*9, 10, 28*). Hypercitrullination not only expands the pool of citrullinated proteins, which can serve as autoantigens of RA, but also facilitates the formation of NETs. NETs are inflammatory in nature and are also a rich source of citrullinated antigens. Our data strongly suggest that hypercitrullination can also further augment the expression of IL-1β
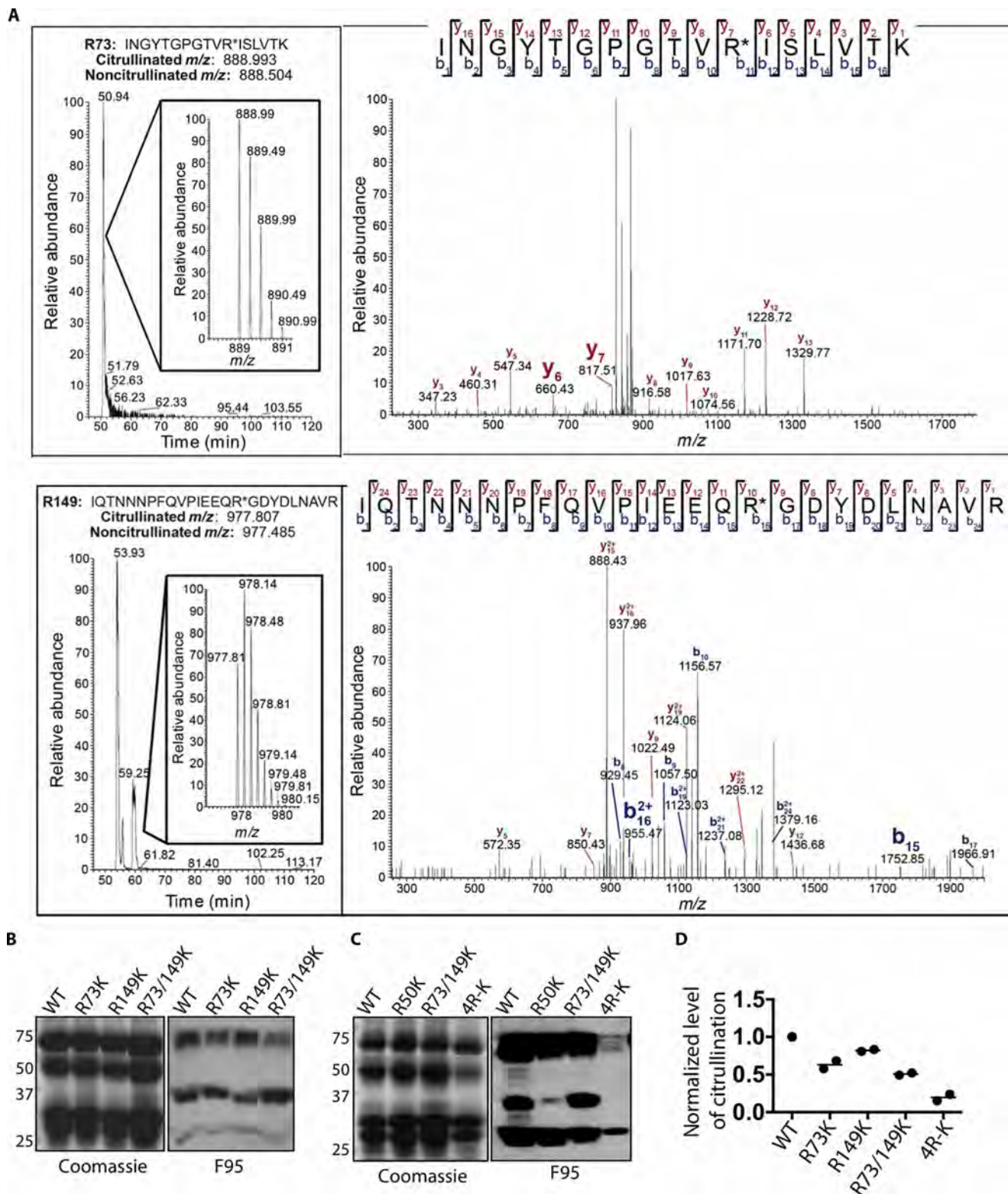
Fig. 6. Identification of citrullination sites within p65. (**A**) Extracted MS1 chromatograms and high-resolution isotope envelops (inset) of the R73 and R149 peptides of cit–GST-p65 are shown at the left panels. Annotated MS2 fragmentation spectra of the citrullinated R73 and R149 peptides are shown at the right panels. (**B** to **D**) Recombinant GST-p65 and indicated R-to-K mutants were citrullinated with PAD4, fractionated in SDS-PAGE gels, stained with Coomassie blue (B and C, left panels), or probed with F95 by Western blotting (B and C, right panels). The density of the citrullinated 50- to 80-kDa bands detected with F95 was normalized against that of the corresponding bands detected with Coomassie blue. The normalized density of WT GST-p65 was arbitrarily set as 1. Cumulated results from two experiments are shown in (D). m/z, mass/charge ratio.
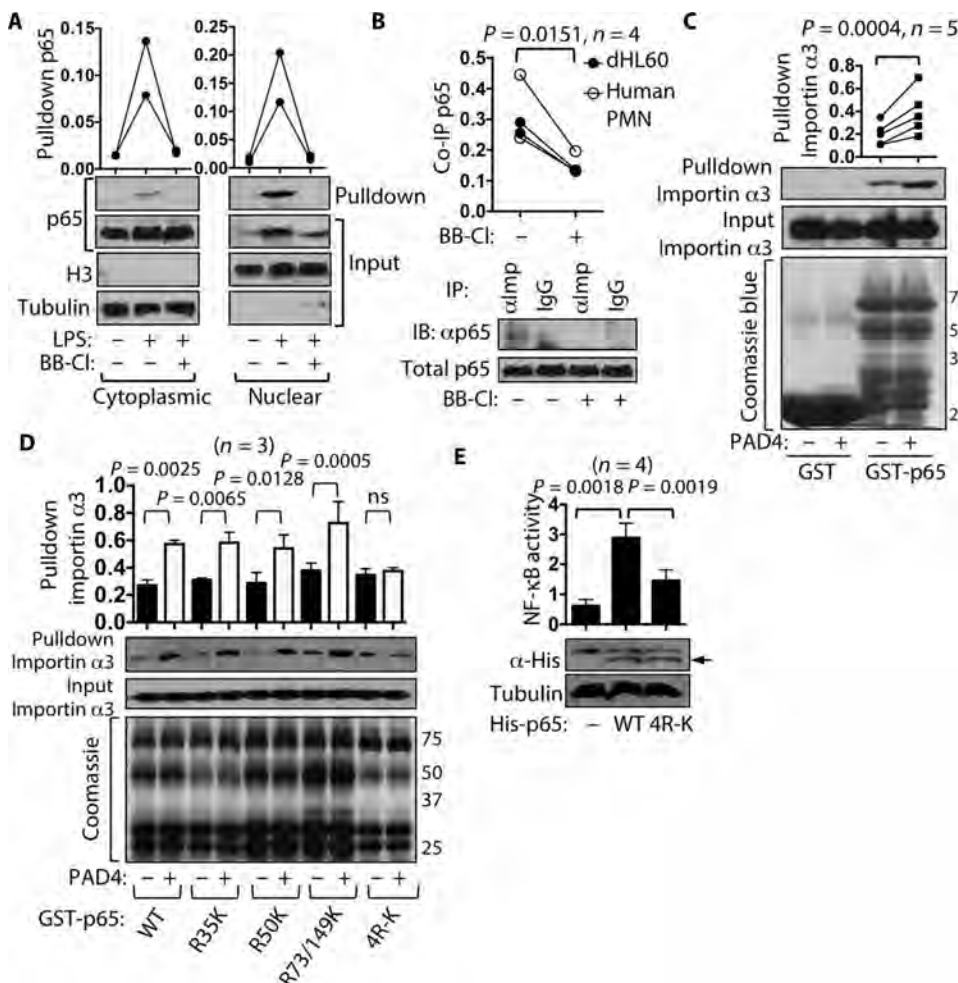
Fig. 7. Augmentation of importin α3/p65 interaction by citrullination of p65. (**A**) Cytoplasmic and nuclear extract was separately prepared from primary human neutrophils stimulated with LPS in the presence or absence of BB-Cl. The detection of cit-p65 was performed according to the methods described in Fig. 5B. Fractions of the biotin-PG–labeled extract before pull down were also analyzed by Western blotting using the indicated antibodies to serve as input controls. The normalized density of cit-p65 from two experiments is shown in the dot graphs. Data points from the same experiments are connected with lines. (**B**) Cell extract from primary human neutrophils (PMN) or dHL60 cells stimulated with LPS in the absence or presence of BB-Cl was subjected to immunoprecipitation with anti–importin α3 (αImp) or control IgG. The immunoprecipitant and a fraction of the unmanipulated extract (total) were probed with anti-p65 by Western blotting. The density of coimmunoprecipitated (Co-IP) p65 was normalized against that of total p65. The normalized density is shown in the dot graph. (**C** and **D**) Recombinant GST (C), GST-p65 (C and D), and indicated R-to-K mutants (D) were incubated or not in vitro with PAD4. A fraction of the recombinant proteins was fractionated on SDS-PAGE gels and stained with Coomassie blue (C and D, bottom panels). The remaining recombinant proteins were used to pull down importin α3 from whole-cell extract prepared from LPS-stimulated dHL60 cells. The pulldown extract and a fraction of unmanipulated dHL60 extract (input) were probed with anti–importin α3 by Western blotting. The normalized density of pulldown importin α3 from at least three independent experiments is shown in the dot graph of (C) and in the bar graph of (D). (**E**) dHL60 cells were transfected with empty vectors (–) or vectors expressing WT or 4R-K His-p65 along with the NF-κB reporter. The normalized luciferase activity (NF-κB activity) is shown in the bar graph. A fraction of the cell extract was probed with indicated antibodies by Western blotting. The arrow marks the location of exogenous His-p65.

and TNFα, thereby propagating joint inflammation. This latter mechanism explains why the type 1 haplotype of *PADI4* increases the risk of RA.

Pan-PAD inhibitors have shown therapeutic effects in animal models of RA and other autoimmune diseases, including inflammatory bowel disease and lupus (*13*, *29*, *30*). The current dogma indicates that the therapeutic effect of the pan-PAD inhibitors comes from their abil-

ity to attenuate the formation of NETs. Because IL-1β and TNFα, two potent inflammatory cytokines, are pathogenic in many of those models, our data provide an additional explanation for the therapeutic effect of PAD inhibition, that is, by suppressing the expression of these two cytokines. As citrullination also critically regulates embryogenesis and the pluripotency of embryonic stem cells, global inhibition of PADs can have unwanted effects. Targeting the interaction between p65 and PADs may enable us to specifically inhibit the citrullination of p65 without the unwanted effects of pan-PAD inhibitors.

MATERIALS AND METHODS
Human patients
Peripheral blood of healthy donors was obtained through the Partners Health-Care Biobank, an enterprise biobank of consented patient samples at Partners HealthCare (Massachusetts General Hospital and Brigham and Women's Hospital), and Brigham and Women's Hospital Specimen Bank according to institutional review board–approved protocols.

Mouse
The generation of PAD2KO and PAD4KO mice was described previously (*6*, *31*). The mice were backcrossed to DBA/1J mice for 12 generations before use. Littermates were used for all experiments

Preparation and stimulation of neutrophils
Human neutrophils were enriched from peripheral blood of healthy donors according to a previously published protocol (*32*). Mouse neutrophils from bone marrow were isolated on a Percoll gradient. Neutrophils were washed and resuspended to 2×10^6/ml in Hanks' balanced salt solution (without Ca^{2+}/Mg^{2+}; Gibco, Thermo Fisher) in the presence of 0.5% heat-inactivated human serum (Sigma-Aldrich), pretreated with BB-Cl (5 to 10 μM) or DMSO for 40 min at 37°C before stimulation with LPS (1 μg/ml; Sigma-Aldrich), GM-CSF (50 ng/ml; BioLegend), or IFNγ (50 ng/ml; BioLegend) for 2 hours.

Real-time PCR
RNA isolation, reverse transcription, and real-time polymerase chain reaction (PCR) were performed as described (*33*). Transcript level thus detected was normalized against that of actin (Fig. 1, B to E, and

figs. S1 and S2) or HPRT (Figs. 1I and 2). The sequences of the primers used are listed in table S2.

In vitro neutrophil bactericidal assay

Pseudomonas aeruginosa strain PAO1 (5×10^6 in 1 μl) was incubated with mouse neutrophils (2×10^6 cells in 1 ml of RPMI) in flat-bottom 24-well plates for 2 hours at 37°C. The wells were treated with 0.01% Triton X-100 for 5 min to lyse neutrophils, and 10 μl of lysate was applied to nutrient agar plates, which were incubated overnight at 37°C. The survival of PAO1 was calculated by the colony number of PAO1 with neutrophil incubation versus the colony number of PAO1 without neutrophil incubation.

LPS-induced acute lung injury

Mice were first injected intraperitoneally with BB-Cl (5 mg/kg) or DMSO and then received an intraperitoneal injection of LPS (5 mg/g of body weight) 4 hours later to induce lung injury. Two hours after the LPS injection, mice were sacrificed. RNA was prepared from lungs using TRIzol (Ambion). In some experiments, bronchoalveolar lavage (BAL) was performed and the number of neutrophils in BAL fluid was counted.

Cell lines, plasmid, mutagenesis, transfection, and luciferase assay

HL60 human promyelocytic leukemia cells were maintained in RPMI medium containing 10% heat-inactivated fetal bovine serum (FBS; HyClone, GE Healthcare Life Science) and 1% (v/v) penicillin-streptomycin (Gibco). Differentiation of HL60 was induced with 1.3% DMSO for 6 to 7 days. 3×NF-κB-Luc, 3×NF-AT-Luc, 3×CRE-Luc, and pTK-Renilla luciferase vector were described previously (*34*). The cDNA of human p65 was cloned into pcDNA3.1/His A vector (Invitrogen). R-to-K mutants of p65 were generated with QuikChange XL Site-Directed Mutagenesis kit (Stratagene) according to the manufacturer's instructions. The primers used are 5′-CAGCCCAAGCAGAAGG-GCATGCGCTTC-3′ (for R30K), 5′-CAGCGGGGCATGAAGTTC-CGCTACAAG-3′ (for R33K), 5′-GGCATGCGCTTCAAGTACAAG-TGCGAG-3′ (for R35K), 5′-AAGTGCGAGGGGAAGTCCGCGGGCAGC-3′ (for R41K), 5′-ATCCCAGGCGAGAAGAGCACAGATACC-3′ (for R50K), 5′-CCAGGGACAGTGAAGATCTCCCTGGTC-3′ (for R73K), and 5′-ATAGAAGAGCAGAAGGGGGACTACGAC-3′ (for R149K). Human PAD4 and SNP-PAD4 cDNA are gifts from A. Rosen (Johns Hopkins Medical Institute) (*35*) and were cloned into pcDNA3.1/HisA plasmid.

Transfection of dHL60 cells was performed with Amaxa Cell Line Nucleofector Kit V (Amaxa Biosystems). The pTK-Renilla luciferase reporter (1 μg) was included in each transfection. Luciferase activity was detected with the Dual-Luciferase Reporter Assay System (Promega) according to the manufacturer's protocol. Values obtained from firefly luciferase signals were normalized to *Renilla* luciferase activity.

Western blotting

The preparation of cell extract was described (*33*). The following antibodies were used: anti-p65 (8242S) and anti–histone H3 (4620S) from Cell Signaling Technology; anti-PAD4 (ab128086), anti-KPNA4 (importin α3; ab176585), and anti–cit-H3 (ab5103) from Abcam; and anti-tubulin (T5168) from Sigma-Aldrich. Densitometry readings of Western blots were obtained with UN-SCAN-IT 6.0 software (Silk Scientific Inc.) and normalized against those of indicated loading controls.

Immunocytochemistry and confocal analysis

dHL60 cells were allowed to settle onto poly-L-lysine–coated glass coverslips for 15 min at 37°C. Coverslips were blocked with 10% FBS, 1% bovine serum albumin, 0.05% Triton X-100, and 2 mM EDTA in phosphate-buffered saline (PBS) overnight. Staining was done with rabbit anti–NF-κB p65 (Cell Signaling, catalog no. 8242S) at 1:100 dilution for 2 hours followed by donkey anti-rabbit IgG-AF594 (Jackson ImmunoResearch). Draq5 (Cell Signaling) was used to stain DNA. Confocal microscopy was performed on a Nikon TE2000-U inverted microscope.

Immunoprecipitation

Cells were lysed in lysis buffer containing 20 mM tris (pH 8.0), 138 mM NaCl, 10% glycerol, 1% NP-40, 10 mM NaF, 2 mM NaVO$_4$, 1 mM pyrophosphoric acid, and CPI (CompleteTM protease inhibitor, Roche Applied Science) and centrifuged at 12,000 rpm at 4°C for 15 min. The supernatant was incubated with indicated antibodies (2 μg per sample) overnight at 4°C and then incubated with Protein A/G PLUS–Agarose (Santa Cruz Biotechnology) for 4 hours at 4°C. The bound proteins were eluted by boiling for 10 min at 1× loading buffer and subjected to Western blotting.

GST pulldown assay

The cDNA of p65 or PAD4 was cloned into pGEX-4T3 or pGEX-6P1 vector (GE Healthcare), respectively, expressed in bacteria (BL21, EMD Millipore) as GST-fused proteins, and prebound to glutathione-agarose beads (Sigma). The full-length and truncation mutants of p65 or PAD4 were subcloned into pcDNA3.1/His A vector (Invitrogen) and expressed in 293T cells. Whole-cell lysate was prepared 48 hours after transfection in lysis buffer containing 20 mM tris (pH 8.0), 138 mM NaCl, 10% glycerol, 1% NP-40, 10 mM NaF, 2 mM NaVO$_4$, 1 mM pyrophosphoric acid, and CPI. The lysate was incubated with GST-p65 or GST-PAD4 bound beads overnight at 4°C. The captured proteins were then eluted and subjected to Western blotting analysis.

Computer modeling of the PAD4/p65 interaction

Protein-protein docking was accomplished by using BioLuminate (Schrodinger Release 2016-3, Schrodinger Inc.), which implements the program PIPER (*36*). PAD4 (PDB ID, 4DKT) and the DNA and dimerization of p65 (PDB ID, 2I9C) were prepared using the Protein Preparation modular in Maestro (*37*). For PAD4, the biological unit was created using crystal symmetry mates, and all crystallographic waters, buffer, and salts were deleted from the structure. The DNA binding and dimerization domains of p65 were extracted from all other molecules present including DNA and p50. Complexes were specifically evaluated for interactions between the N terminus of PAD4 and p65. The first complex where this interaction was observed was energy-minimized using Prime (*38*) with the OPLS3 force field (*39*).

Detection of in vivo cit-p65

Whole-cell lysates were prepared by sonication in Branson Sonifier 250 (Emerson Electric) in a buffer containing 50 mM Hepes. Citrullinated proteins were labeled with biotin-PG (0.1 mM) in a buffer containing 50 mM Hepes and 20% trichloroacetic acid at 37°C for 30 min. After centrifuge, the pellet was resuspended in PBS containing 0.25% SDS, 0.14% β-mercaptoethanol, 0.4 mM Hepes, 2 mM arginine, and 2 mM NaCl. Biotin-PG–labeled citrullinated proteins were captured with streptavidin-agarose beads (Thermo Fisher) overnight at 4°C. The captured proteins were subjected to Western blotting.

In vitro citrullination

Soluble GST-p65 fusion protein was incubated with purified recombinant PAD4 (10 mM) in a buffer containing 100 mM Hepes, 100 mM NaCl, 10 mM CaCl$_2$, 0.1 mM EDTA, and 2 mM dithiothreitol for 4 hours at 37°C. After washing with PBS, the beads were boiled for 10 min and subjected to Western blotting. The cit-p65 was detected with F95 antibody.

Identification of citrullination sites by LC-MS/MS

In-gel digestion was performed according to a published protocol (40). LC-MS/MS analysis was performed on an LTQ Orbitrap Discovery mass spectrometer (Thermo Fisher) coupled to an Agilent 1200 series HPLC. Samples were pressure-loaded onto a hand-pulled 100-μm fused-silica capillary column with a 5-μm tip packed with a 10-cm Aqua C18 reverse phase resin (Phenomenex). Peptides were eluted using a 3-hour gradient of 0 to 100% buffer B in buffer A (buffer A: 95% water, 5% acetonitrile, 0.1% formic acid; buffer B: 20% water, 80% acetonitrile, 0.1% formic acid). The flow rate through the column was set to ~0.25 μl/min, and the spray voltage was set to 2.75 kV. One full MS scan (FTMS) was followed by seven data-dependent scans (ITMS) of the seven most abundant ions. For high-resolution runs, a full scan (FTMS) was followed by four data-dependent scans (FTMS) limited to an inclusion mass list containing the masses of previously identified citrullinated peptides.

The tandem MS data were searched with the SEQUEST algorithm using a concatenated target/decoy variant of the human UniProt database. A static modification of +57.02146 on cysteine was specified to account for alkylation by iodoacetamide, and a differential modification of 0.984 was specified on arginine. SEQUEST output files were filtered using DTASelect.

Statistical analysis

Statistical analysis was performed using Student's t test (Figs. 2, E and F, 3, E and F, and 7, B and C) or one-way analysis of variance (ANOVA) (Figs. 1, B, C, and I, 2, A, C, D, and G to I, 3, A, C, and D, and 7, D and E). All bar graphs shown are means and SD. Multiple comparisons were also performed after one-way ANOVA if it was statistically significant. The P values of two-sided Student's t test (two-sided) and multiple comparisons in one-way ANOVA are shown. n stands for the number of biological replicate, except in Fig. 1 (F and H), where n represents the number of technical replicate.

SUPPLEMENTARY MATERIALS

immunology.sciencemag.org/cgi/content/full/2/12/eaal3062/DC1
Fig. S1. Impacts of BB-Cl on neutrophils.
Fig. S2. Functional redundancy between PAD2 and PAD4.
Fig. S3. Immunocytochemistry of dHL60 cells.
Fig. S4. Preparation of native and cit–GST-p65 for MS.
Fig. S5. 4R-K mutant does not affect the interaction between p65 and PAD4.
Fig. S6. Citrullination of p65 does not attenuate its binding to the IL-1β NF-κB site.
Table S1. Spectral counts and charge states for citrullinated peptides identified in gel band extractions of citrullinated and native GST-p65 via LC-MS/MS.
Table S2. Sequence of primers used in real-time PCR.
Source data Excel file
Source data blots

REFERENCES AND NOTES

1. K. L. Bicker, P. R. Thompson, The protein arginine deiminases: Structure, function, inhibition, and disease. *Biopolymers* **99**, 155–163 (2013).
2. E. Darrah, A. Rosen, J. T. Giles, F. Andrade, Peptidylarginine deiminase 2, 3 and 4 have distinct specificities against cellular substrates: Novel insights into autoantigen selection in rheumatoid arthritis. *Ann. Rheum. Dis.* **71**, 92–98 (2012).
3. G. Esposito, A. M. Vitale, F. P. J. Leijten, A. M. Strik, A. M. C. B. Koonen-Reemst, P. Yurttas, T. J. A. A. Robben, S. Coonrod, J. A. Gossen, Peptidylarginine deiminase (PAD) 6 is essential for oocyte cytoskeletal sheet formation and female fertility. *Mol. Cell. Endocrinol.* **273**, 25–31 (2007).
4. M. A. Christophorou, G. Castelo-Branco, R. P. Halley-Stott, C. S. Oliveira, R. Loos, A. Radzisheuskaya, K. A. Mowen, P. Bertone, J. C. Silva, M. Zernicka-Goetz, M. L. Nielsen, J. B. Gurdon, T. Kouzarides, Citrullination regulates pluripotency and histone H1 binding to chromatin. *Nature* **507**, 104–108 (2014).
5. S. C. Stadler, C. T. Vincent, V. D. Fedorov, A. Patsialou, B. D. Cherrington, J. J. Wakshlag, S. Mohanan, B. M. Zee, X. Zhang, B. A. Garcia, J. S. Condeelis, A. M. Brown, S. A. Coonrod, C. D. Allis, Dysregulation of PAD4-mediated citrullination of nuclear GSK3β activates TGF-β signaling and induces epithelial-to-mesenchymal transition in breast cancer cells. *Proc. Natl. Acad. Sci. U.S.A.* **110**, 11851–11856 (2013).
6. P. Li, M. Li, M. R. Lindberg, M. J. Kennett, N. Xiong, Y. Wang, PAD4 is essential for antibacterial innate immunity mediated by neutrophil extracellular traps. *J. Exp. Med.* **207**, 1853–1862 (2010).
7. P. Proost, T. Loos, A. Mortier, E. Schutyser, M. Gouwy, S. Noppen, C. Dillen, I. Ronsse, R. Conings, S. Struyf, G. Opdenakker, P. C. Maudgal, J. Van Damme, Citrullination of CXCL8 by peptidylarginine deiminase alters receptor usage, prevents proteolysis, and dampens tissue inflammation. *J. Exp. Med.* **205**, 2085–2097 (2008).
8. M. K. Demoruelle, K. Deane, Antibodies to citrullinated protein antigens (ACPAs): Clinical and pathophysiologic significance. *Curr. Rheumatol. Rep.* **13**, 421–430 (2011).
9. D. Makrygiannakis, M. Hermansson, A.-K. Ulfgren, A. P. Nicholas, A. J. Zendman, A. Eklund, J. Grunewald, C. M. Skold, L. Klareskog, A. I. Catrina, Smoking increases peptidylarginine deiminase 2 enzyme expression in human lungs and increases citrullination in BAL cells. *Ann. Rheum. Dis.* **67**, 1488–1492 (2008).
10. H.-H. Chang, N. Dwivedi, A. P. Nicholas, I.-C. Ho, The W620 polymorphism in PTPN22 disrupts its interaction with peptidylarginine deiminase type 4 and enhances citrullination and NETosis. *Arthritis Rheumatol.* **67**, 2323–2334 (2015).
11. S. Viatte, D. Plant, S. Raychaudhuri, Genetics and epigenetics of rheumatoid arthritis. *Nat. Rev. Rheumatol.* **9**, 141–153 (2013).
12. R. Khandpur, C. Carmona-Rivera, A. Vivekanandan-Giri, A. Gizinski, S. Yalavarthi, J. S. Knight, S. Friday, S. Li, R. M. Patel, V. Subramanian, P. Thompson, P. Chen, D. A. Fox, S. Pennathur, M. J. Kaplan, NETs are a source of citrullinated autoantigens and stimulate inflammatory responses in rheumatoid arthritis. *Sci. Transl. Med.* **5**, 178ra140 (2013).
13. J. S. Knight, V. Subramanian, A. A. O'Dell, S. Yalavarthi, W. Zhao, C. K. Smith, J. B. Hodgin, P. R. Thompson, M. J. Kaplan, Peptidylarginine deiminase inhibition disrupts NET formation and protects against kidney, skin and vascular disease in lupus-prone MRL/*lpr* mice. *Ann. Rheum. Dis.* **74**, 2199–2206 (2015).
14. I. Neeli, N. Dwivedi, S. Khan, M. Radic, Regulation of extracellular chromatin release from neutrophils. *J. Innate Immun.* **1**, 194–201 (2009).
15. B. Sun, X. Hu, G. Liu, B. Ma, Y. Xu, T. Yang, J. Shi, F. Yang, H. Li, L. Zhang, Y. Zhao, Phosphatase Wip1 negatively regulates neutrophil migration and inflammation. *J. Immunol.* **192**, 1184–1195 (2014).
16. P. Xia, S. Wang, B. Ye, Y. Du, G. Huang, P. Zhu, Z. Fan, Sox2 functions as a sequence-specific DNA sensor in neutrophils to initiate innate immunity against microbial infection. *Nat. Immunol.* **16**, 366–375 (2015).
17. Y. Wang, J. Wysocka, J. Sayegh, Y.-H. Lee, J. R. Perlin, L. Leonelli, L. S. Sonbuchner, C. H. McDonald, R. G. Cook, Y. Dou, R. G. Roeder, S. Clarke, M. R. Stallcup, C. D. Allis, S. A. Coonrod, Human PAD4 regulates histone arginine methylation levels via demethylimination. *Science* **306**, 279–283 (2004).
18. A. Suzuki, R. Yamada, X. Chang, S. Tokuhiro, T. Sawada, M. Suzuki, M. Nagasaki, M. Nakayama-Hamada, R. Kawaida, M. Ono, M. Ohtsuki, H. Furukawa, S. Yoshino, M. Yukioka, S. Tohma, T. Matsubara, S. Wakitani, R. Teshima, Y. Nishioka, A. Sekine, A. Iida, A. Takahashi, T. Tsunoda, Y. Nakamura, K. Yamamoto, Functional haplotypes of *PADI4*, encoding citrullinating enzyme peptidylarginine deiminase 4, are associated with rheumatoid arthritis. *Nat. Genet.* **34**, 395–402 (2003).
19. N. Horikoshi, H. Tachiwana, K. Saito, A. Osakabe, M. Sato, M. Yamada, S. Akashi, Y. Nishimura, W. Kagawa, H. Kurumizaka, Structural and biochemical analyses of the human PAD4 variant encoded by a functional haplotype gene. *Acta Crystallogr. D Biol. Crystallogr.* **67**, 112–118 (2011).
20. J. L. Slack, L. E. Jones Jr., M. M. Bhatia, P. R. Thompson, Autodeimination of protein arginine deiminase 4 alters protein–protein interactions but not activity. *Biochemistry* **50**, 3997–4010 (2011).
21. K. L. Bicker, V. Subramanian, A. A. Chumanevich, L. J. Hofseth, P. R. Thompson, Seeing citrulline: Development of a phenylglyoxal-based probe to visualize protein citrullination. *J. Am. Chem. Soc.* **134**, 17015–17018 (2012).
22. A. P. Nicholas, J. N. Whitaker, Preparation of a monoclonal antibody to citrullinated epitopes: Its characterization and some applications to immunohistochemistry in human brain. *Glia* **37**, 328–336 (2002).
23. R. Fagerlund, L. Kinnunen, M. Köhler, I. Julkunen, K. Melén, NF-κB is transported into the nucleus by importin α3 and importin α4. *J. Biol. Chem.* **280**, 15942–15951 (2005).

24. M. M. Rabadi, M. Kim, V. D. D'Agati, H. T. Lee, Peptidyl arginine deiminase-4 deficient mice are protected against kidney and liver injury after renal ischemia and reperfusion. *Am. J. Physiol. Renal Physiol.* **311**, F437–F449 (2016).

25. P. Sharma, S. Azebi, P. England, T. Christensen, A. Moller-Larsen, T. Petersen, E. Batsche, C. Muchardt, Citrullination of histone H3 interferes with HP1-mediated transcriptional repression. *PLOS Genet.* **8**, e1002934 (2012).

26. F. Ghari, A. M. Quirke, S. Munro, J. Kawalkowska, S. Picaud, J. McGouran, V. Subramanian, A. Muth, R. Williams, B. Kessler, P. R. Thompson, P. Fillipakopoulos, S. Knapp, P. J. Venables, N. B. La Thangue, Citrullination-acetylation interplay guides E2F-1 activity during the inflammatory response. *Sci. Adv.* **2**, e1501257 (2016).

27. H. J. Lee, M. Joo, R. Abdolrasulnia, D. G. Young, I. Choi, L. B. Ware, T. S. Blackwell, B. W. Christman, Peptidylarginine deiminase 2 suppresses inhibitory κB kinase activity in lipopolysaccharide-stimulated RAW 264.7 macrophages. *J. Biol. Chem.* **285**, 39655–39662 (2010).

28. H.-H. Chang, G.-Y. Liu, N. Dwivedi, B. Sun, Y. Okamoto, J. D. Kinslow, K. D. Deane, M. K. Demoruelle, J. M. Norris, P. R. Thompson, J. A. Sparks, D. A. Rao, E. W. Karlson, H.-C. Hung, V. M. Holers, I.-C. Ho, A molecular signature of preclinical rheumatoid arthritis triggered by dysregulated PTPN22. *JCI Insight* **1**, e90045 (2016).

29. V. C. Willis, A. M. Gizinski, N. K. Banda, C. P. Causey, B. Knuckley, K. N. Cordova, Y. Luo, B. Levitt, M. Glogowska, P. Chandra, L. Kulik, W. H. Robinson, W. P. Arend, P. R. Thompson, V. M. Holers, N-α-benzoyl-N5-(2-chloro-1-iminoethyl)-L-ornithine amide, a protein arginine deiminase inhibitor, reduces the severity of murine collagen-induced arthritis. *J. Immunol.* **186**, 4396–4404 (2011).

30. A. A. Chumanevich, C. P. Causey, B. A. Knuckley, J. E. Jones, D. Poudyal, A. P. Chumanevich, T. Davis, L. E. Matesic, P. R. Thompson, L. J. Hofseth, Suppression of colitis in mice by Cl-amidine: A novel peptidylarginine deiminase inhibitor. *Am. J. Physiol. Gastrointest. Liver Physiol.* **300**, G929–G938 (2011).

31. R. Raijmakers, J. Vogelzangs, J. Raats, M. Panzenbeck, M. Corby, H. Jiang, M. Thibodeau, N. Haynes, W. J. Van Venrooij, G. J. M. Pruijn, B. Werneburg, Experimental autoimmune encephalomyelitis induction in peptidylarginine deiminase 2 knockout mice. *J. Comp. Neurol.* **498**, 217–226 (2006).

32. I. Neeli, S. N. Khan, M. Radic, Histone deimination as a response to inflammatory stimuli in neutrophils. *J. Immunol.* **180**, 1895–1902 (2008).

33. H.-H. Chang, S.-C. Miaw, W. Tseng, Y.-W. Sun, C.-C. Liu, H.-W. Tsao, I.-C. Ho, PTPN22 modulates macrophage polarization and susceptibility to dextran sulfate sodium–induced colitis. *J. Immunol.* **191**, 2134–2143 (2013).

34. B. Y. Kang, S.-C. Miaw, I.-C. Ho, ROG negatively regulates T-cell activation but is dispensable for Th-cell differentiation. *Mol. Cell. Biol.* **25**, 554–562 (2005).

35. M. L. Harris, E. Darrah, G. K. Lam, S. J. Bartlett, J. T. Giles, A. V. Grant, P. Gao, W. W. Scott Jr., H. El-Gabalawy, L. Casciola-Rosen, K. C. Barnes, J. M. Bathon, A. Rosen, Association of autoimmunity to peptidyl arginine deiminase type 4 with genotype and disease severity in rheumatoid arthritis. *Arthritis Rheum.* **58**, 1958–1967 (2008).

36. D. Kozakov, R. Brenke, S. R. Comeau, S. Vajda, PIPER: An FFT-based protein docking program with pairwise potentials. *Proteins* **65**, 392–406 (2006).

37. G. M. Sastry, M. Adzhigirey, T. Day, R. Annabhimoju, W. Sherman, Protein and ligand preparation: Parameters, protocols, and influence on virtual screening enrichments. *J. Comput. Aided Mol. Des.* **27**, 221–234 (2013).

38. M. P. Jacobson, D. L. Pincus, C. S. Rapp, T. J. F. Day, B. Honig, D. E. Shaw, R. A. Friesner, A hierarchical approach to all-atom protein loop prediction. *Proteins* **55**, 351–367 (2004).

39. E. Harder, W. Damm, J. Maple, C. Wu, M. Reboul, J. Y. Xiang, L. Wang, D. Lupyan, M. K. Dahlgren, J. L. Knight, J. W. Kaus, D. S. Cerutti, G. Krilov, W. L. Jorgensen, R. Abel, R. A. Friesner, OPLS3: A force field providing broad coverage of drug-like small molecules and proteins. *J. Chem. Theory Comput.* **12**, 281–296 (2016).

40. M. M. Dix, G. M. Simon, B. F. Cravatt, Global mapping of the topography and magnitude of proteolytic events in apoptosis. *Cell* **134**, 679–691 (2008).

Science Immunology

Citrullination of NF-κB p65 promotes its nuclear localization and TLR-induced expression of IL-1 β and TNFα

Bo Sun, Nishant Dwivedi, Tyler J. Bechtel, Janet L. Paulsen, Aaron Muth, Mandar Bawadekar, Gang Li, Paul R. Thompson, Miriam A. Shelef, Celia A. Schiffer, Eranthie Weerapana and I-Cheng Ho

PADs inflame arthritis

Individuals with rheumatoid arthritis (RA) produce an autoimmune response to citrullinated proteins that may contribute to disease pathology. Sun *et al.* report that citrullination also directly contributes to RA-associated inflammation. They found that decreased activity of peptidylarginine deiminases (PADs), which catalyze peptide citrullination, limited TLR-induced expression of the proinflammatory cytokines IL-1β and TNFα by neutrophils. PAD4 directly citrullinated the proinflammatory signaling molecule NF- κB p65, enhancing transport into the nucleus. An RA-associated human variant of PAD4 interacted more closely with NF- κB p65, thereby augmenting NF-κB activity. These data suggest that the interaction between PADs and NF- κB p65 may serve as a more specific target to treat RA.

ARTICLE TOOLS	http://immunology.sciencemag.org/content/2/12/eaal3062
SUPPLEMENTARY MATERIALS	http://immunology.sciencemag.org/content/suppl/2017/06/06/2.12.eaal3062.DC1
REFERENCES	This article cites 40 articles, 15 of which you can access for free http://immunology.sciencemag.org/content/2/12/eaal3062#BIBL
PERMISSIONS	http://www.sciencemag.org/help/reprints-and-permissions

Use of this article is subject to the Terms of Service